

1 **Research article**

2 **Title**

3 Spatial variations in terrestrial net ecosystem productivity and its local indicators

4 **Running title**

5 Spatial variability in terrestrial NEP

6 **Authors**

7 Erqian Cui^{1,2} (eqcui@stu.ecnu.edu.cn)

8 Chenyu Bian^{1,2} (cybian@stu.ecnu.edu.cn)

9 Yiqi Luo³ (yiqi.luo@nau.edu)

10 Shuli Niu^{4,5} (sniu@igsnr.ac.cn)

11 Yingping Wang⁶ (Yingping.Wang@csiro.au)

12 Jianyang Xia^{1,2,*} (jyxia@des.ecnu.edu.cn)

13 **Affiliations**

14 ¹Zhejiang Tiantong Forest Ecosystem National Observation and Research Station, Shanghai
15 Key Lab for Urban Ecological Processes and Eco-Restoration, School of Ecological and
16 Environmental Sciences, East China Normal University, Shanghai 200241, China;

17 ²Research Center for Global Change and Ecological Forecasting, East China Normal University,
18 Shanghai 200241, China;

19 ³Center for ecosystem science and society, Northern Arizona University, Arizona, Flagstaff, AZ
20 86011, USA.

21 ⁴Key Laboratory of Ecosystem Network Observation and Modeling, Institute of Geographic
22 Sciences and Natural Resources Research, Chinese Academy of Sciences, Beijing, China;

23 ⁵University of Chinese Academy of Sciences, Beijing, China;

24 ⁶CSIRO Oceans and Atmosphere, PMB 1, Aspendale, Victoria 3195, Australia.

25 **Correspondence**

26 Jianyang Xia, School of Ecological and Environmental Sciences, East China Normal University,
27 Shanghai 200241, China.

28 Email: jyxia@des.ecnu.edu.cn

29 **Key words**

30 Net ecosystem productivity, spatial variation, net CO₂ uptake and release, local indicators,
31 model

32 **Abstract**

33 Multiple lines of evidence have demonstrated the persistence of global land carbon (C) sink
34 during the past several decades. However, both annual net ecosystem productivity (NEP) and
35 its inter-annual variation (IAV_{NEP}) keep varying over space. Thus, identifying local indicators
36 for the spatially varying NEP and IAV_{NEP} is critical for locating the major and sustainable C
37 sinks on the land. Here, based on daily NEP observations from FLUXNET sites and large-scale
38 estimates from an atmospheric inversion product, we found a robust logarithmic correlation
39 between annual NEP and seasonal carbon uptake-release ratio (i.e., U/R). The cross-site
40 variation of mean annual NEP could be logarithmically indicated by U/R , while the spatial
41 distribution of IAV_{NEP} was associated with the slope (i.e., β) of the logarithmic correlation
42 between annual NEP and U/R . Among biomes, for example, forests and croplands had the largest
43 U/R ratio (1.06 ± 0.83) and β ($473 \pm 112 \text{ g C m}^{-2} \text{ yr}^{-1}$), indicating the highest NEP and IAV_{NEP}
44 in forests and croplands, respectively. We further showed that these two simple indicators could
45 directly infer the spatial variations of NEP and IAV_{NEP} in global gridded NEP products. Overall,
46 this study provides two simple local indicators for the intricate spatial variations in the strength
47 and stability of land C sinks. These indicators could be helpful for locating the persistent
48 terrestrial C sinks and provides valuable constraints for improving the simulation of land-
49 atmospheric C exchanges.

50

51 **1. Introduction**

52 Terrestrial ecosystems reabsorb about one-quarter of anthropogenic CO₂ emission (Ciais et
53 al., 2019) and are primarily responsible for the recent temporal fluctuations of the measured
54 atmospheric CO₂ growth rate (Randerson, 2013; Le Quéré et al., 2018). In addition, evidence
55 based on eddy-flux measurements (Baldocchi et al., 2018; Rödenbeck et al., 2018), aircraft
56 atmospheric budgets (Peylin et al., 2013), and process-based model simulations (Poulter et al.,
57 2014; Ahlstrom et al., 2015) has shown a large spatial variability in net ecosystem productivity
58 (NEP) on the land. The elusive variation of terrestrial NEP over space refers to both of the
59 substantial varying mean annual NEP and the divergent inter-annual variability (IAV) in NEP
60 (i.e., IAV_{NEP}; usually quantified as the standard deviation of annual NEP) across space
61 (Baldocchi et al., 2018; Marcolla et al., 2017). The mean annual NEP is related to the strength
62 of carbon exchange of a specific ecosystem (Randerson et al., 2002; Luo and Weng, 2011; Jung
63 et al., 2017), while IAV_{NEP} characterizes the stability of such carbon exchange (Musavi et al.,
64 2017). Thus, whether and how NEP and IAV_{NEP} change over the space is important for
65 predicting the future locations of carbon sinks on the land (Yu et al., 2014; Niu et al., 2017).

66 Large spatial difference in terrestrial NEP has been reported from eddy-flux measurements,
67 model outputs and atmospheric inversion products. In addition, the global average IAV of NEP
68 is large relative to global annual mean NEP (Baldocchi et al., 2018). More importantly, the
69 spatial variations of NEP and IAV_{NEP} have been typically underestimated by the global flux
70 tower-based product and the process-based global models (Jung et al., 2020; Fu et al., 2019).
71 These discrepancies have further revealed the necessary to identify local indicators for the
72 spatially varying NEP and IAV_{NEP}, separately. The NEP in terrestrial ecosystems is determined
73 by two components, including vegetation photosynthesis and ecosystem respiration (Reichstein
74 et al., 2005), and their relative difference could determine the spatial variation of NEP
75 (Baldocchi et al., 2015; Biederman et al., 2016). Many previous analyses have attributed the
76 IAV_{NEP} at the site level to the different sensitivities of ecosystem photosynthesis and respiration
77 to environmental drivers (Gilmanov et al., 2005; Reichstein et al., 2005) and biotic controls
78 (Besnard et al., 2018; Musavi et al., 2017). For example, some studies have reported that IAV_{NEP}
79 is more associated with variations in photosynthesis than carbon release (Ahlstrom et al., 2015;

80 Novick et al., 2015; Li et al., 2017), whereas others have indicated that respiration is more
81 sensitive to anomalous climate variability (Valentini et al., 2000; von Buttlar et al., 2017).
82 However, despite the previous efforts in a predictive understanding of the land-atmospheric C
83 exchanges, the multi-model spread has not reduced over time (Arora et al., 2019). Therefore, it
84 is imperative to explore the potential indicators for the spatially varying NEP, which could help
85 attribute the spatial variation of NEP and IAV_{NEP} into different processes and provide valuable
86 constraints for the global C cycle. Alternatively, the annual NEP of a given ecosystem can be
87 also directly decomposed into net CO₂ uptake flux and CO₂ release flux (Gray et al., 2014),
88 which are more direct components for NEP (Fu et al., 2019). It is still unclear how the ecosystem
89 net CO₂ uptake and release fluxes would control the spatially varying NEP.

90 Conceptually, the total net CO₂ uptake flux (U) is determined by the length of CO₂ uptake
91 period (CUP) and the CO₂ uptake rate, while the total net CO₂ release flux (R) depends on the
92 length of CO₂ release period (CRP) and the CO₂ release rate (Fig. 1b). The variations of NEP
93 thus could be attributed to these decomposed components. A strong spatial correlation between
94 mean annual NEP and length of CO₂ uptake period has been reported in evergreen needle- and
95 broad-leaved forests (Churkina et al., 2005; Richardson et al., 2013; Keenan et al., 2014),
96 whereas atmospheric inversion data and vegetation photosynthesis model indicated a dominant
97 role of the maximal carbon uptake rate (Fu et al., 2017; Zhou et al., 2017). However, the relative
98 importance of these phenological and physiological indicators for the spatially varying NEP
99 remains unclear.

100 In this study, we decomposed annual NEP into U and R , and explored the local indicators
101 for spatially varying NEP. Based on the eddy-covariance fluxes from FLUXNET2015 Dataset
102 (Pastorello et al., 2017) and the atmospheric inversion product (Rödenbeck et al., 2018), we
103 examined the relationship between NEP and its direct components. In addition, we used the
104 observations to evaluate the spatial variations of NEP and IAV_{NEP} in the FLUXCOM product
105 and a process-based model (CLM4.5) (Oleson et al., 2013). The major aim of this study is to
106 explore whether there are useful local indicators for the spatially varying NEP and IAV_{NEP} in
107 terrestrial ecosystems.

108 **2. Materials and Methods**

109 **2.1 Datasets**

110 Daily NEP observations of eddy covariance sites are obtained from the FLUXNET2015 Tier 1
111 dataset. The FLUXNET2015 dataset provides half-hourly data of carbon, water and energy
112 fluxes at over 210 sites that are standardized and gap-filled (Pastorello et al., 2017). However,
113 time series of most sites are still too short for the analysis of inter-annual variation in NEP. So
114 only the sites that provided the availability of eddy covariance flux measurements for at least 5
115 years are selected. This leads to a global dataset of 72 sites with different biomes across different
116 climatic regions. Based on the biome classification from the International Geosphere-Biosphere
117 Programme (IGBP) provided for the FLUXNET2015 sites, the selected sites include 35 forests
118 (FOR), 15 grasslands (GRA), 11 croplands (CRO), 4 wetlands (WET), 2 shrublands (SHR) and
119 5 savannas (SAV) (Fig. S1 and Table S1).

120 The Jena CarboScope Inversion product combines high precision measurements of
121 atmospheric CO₂ concentration with simulated atmospheric transport to infer the net CO₂
122 exchanges between land, ocean and atmosphere at large scales (Rödenbeck et al., 2018). Here,
123 we used the daily land-atmosphere CO₂ fluxes from the s85_v4.1 version at a spatial resolution
124 of 5° × 3.75°. Considering the relatively low spatial resolution of the Jena Inversion product,
125 the daily fluxes were only used to calculate the local indicators for the spatially varying NEP at
126 the global scale.

127 Daily NEP simulations from Community Land Model version 4.5 (CLM4.5) were also used
128 to calculate the local indicators for the spatially varying NEP at the corresponding flux tower
129 sites. We ran the CLM4.5 model from 1985 to 2010 at a spatial resolution of 1° with CRUNCEP
130 meteorological forcing. Here, NEP was derived as the difference between GPP and TER, and
131 TER was calculated as the sum of simulated autotrophic and heterotrophic respiration. The daily
132 outputs from CLM4.5 were used to calculate the local indicators for the spatially varying NEP
133 both at the global scale and at the FLUXNET site level.

134 The FLUXCOM product presents an upscaling of carbon flux estimates from 224 flux
135 tower sites based on multiple machine learning algorithms and meteorological drivers (Jung et
136 al., 2017). To be consistent with the meteorological forcing of Jena Inversion product and the
137 CLM4.5 model, we used the FLUXCOM CRUNCEPv6 products. In addition, in order to reduce

138 the uncertainty caused by machine-learning methods, we averaged all the FLUXCOM
 139 CRUNCEPv6 products with different machine-learning methods. It should be noted that the
 140 inter-annual variability of FLUXCOM product is driven by meteorological measurements and
 141 satellite data, which partially includes information on vegetation state and other land surface
 142 properties. Daily outputs from FLUXCOM for the period 1985-2010 at 0.5° spatial resolution
 143 were used to calculate the local indicators for the spatially varying NEP both at the global scale
 144 and at the FLUXNET site level.

145 **2.2 Decomposition of NEP and the calculations for its local indicators**

146 The annual NEP of a given ecosystem can be defined numerically as the difference between the
 147 net CO₂ uptake and release (Figure 2b). These components of NEP contain both photosynthesis
 148 and respiration flux, which directly indicate the net CO₂ exchange of an ecosystem. The total
 149 net CO₂ uptake flux (U) and the total net CO₂ release flux (R) can be further decomposed as:

$$150 \quad U = \bar{U} \times CUP \quad (1)$$

$$151 \quad R = \bar{R} \times CRP \quad (2)$$

152 where CUP (d yr⁻¹) is the length of CO₂ uptake period and CRP (d yr⁻¹) is the length of CO₂
 153 release period; \bar{U} (g C m⁻² d⁻¹) is the mean daily net CO₂ uptake over CUP and \bar{R} (g C m⁻² d⁻¹)
 154 represents the mean daily net CO₂ release over CRP . Many studies have reported that the
 155 vegetation net CO₂ uptake during the growing season and the non-growing season soil net CO₂
 156 release are tightly correlated (Luo et al., 2014; Zhao et al., 2016). Therefore, we further tested
 157 the relationship between annual NEP and $\frac{U}{R}$ (i.e., $NEP \propto \frac{U}{R}$), which reflects the seasonal
 158 carbon uptake-release ratio. Consequently, NEP in any given ecosystem can be expressed as
 159 (Fig. S2):

$$160 \quad NEP = \beta \cdot \ln\left(\frac{U}{R}\right) \quad (3)$$

161 where the parameter β represents the slope of the linear relationship of $NEP \propto \ln\left(\frac{U}{R}\right)$,
 162 indicating the site-level carbon uptake sensitivity. Based on the definitions of U and R , the ratio
 163 $\frac{U}{R}$ can be further written as:

164
$$\frac{U}{R} = \frac{\bar{U}}{\bar{R}} \cdot \frac{CUP}{CRP} \quad (4)$$

165 The ratio of $\frac{\bar{U}}{\bar{R}}$ reflects the relative physiological difference between ecosystem CO₂
 166 uptake and release strength, while the ratio of $\frac{CUP}{CRP}$ is an indicator of net ecosystem CO₂
 167 exchange phenology. Environmental changes may regulate these ecological processes and
 168 ultimately affect the ecosystem NEP. The slope β indicates the response sensitivity of NEP to
 169 the changes in phenology and physiological processes. All of β , $\frac{CUP}{CRP}$ and $\frac{\bar{U}}{\bar{R}}$ were then
 170 calculated from the selected eddy covariance sites and the corresponding pixels of these sites in
 171 models. These derived indicators from eddy covariance sites were then used to benchmark the
 172 results extracted from the same locations in models.

173 **2.4 Calculation of the relative contributions**

174 We further quantified the relative contributions of $\frac{\bar{U}}{\bar{R}}$ and $\frac{CUP}{CRP}$ in driving the spatial variations
 175 in NEP:

176
$$NEP = \beta \cdot \left[\ln\left(\frac{\bar{U}}{\bar{R}}\right) + \ln\left(\frac{CUP}{CRP}\right) \right] \quad (5)$$

177 For each eddy covariance site, the parameter β was constant. Then, we used a relative
 178 importance analysis method to quantify the relative contributions of these two ratios to the
 179 spatial variations in NEP. The algorithm was performed with the “ralaimpo” package in R (R
 180 Development Core Team, 2011). The “relaimpo” package is based on variance decomposition
 181 for multiple linear regression models. We chose the most commonly used method named
 182 “Lindeman-Merenda-Gold (LMG)” (Grömping, 2007) from the methods provided by the
 183 “ralaimpo” package. This method allows us to quantify the contributions of explanatory
 184 variables in a multiple linear regression model. Across the 72 FLUXNET sites, we quantified
 185 the relative importance of $\frac{\bar{U}}{\bar{R}}$ and $\frac{CUP}{CRP}$ to cross-site changes in NEP.

186 **3. Results**

187 **3.1 The relationship between NEP and its direct components**

188 To find local indicators for the spatially varying NEP in terrestrial ecosystems, we tested the

189 relationship between NEP and its direct components (U and R) across the 72 flux-tower sites.
190 The results showed that annual NEP was closely related to the ratio $\frac{U}{R}$ (Fig. S2). The
191 logarithmic correlations between annual NEP and $\frac{U}{R}$ were significant at all sites (Fig. 1a), and
192 $\sim 90\%$ of R^2 falling within a range from 0.7 to 1 (Fig. 1c).

193 In addition, the relationship between NEP and $\frac{U}{R}$ was also confirmed by the atmospheric
194 inversion product (i.e., Jena CarboScope Inversion). The control of $\frac{U}{R}$ on annual NEP was
195 robust in most global grid cells (i.e. $0.6 < R^2 < 1$). The coefficient of determination for this
196 relationship was higher in 80% of the regions, but lower in North America (Fig. 2). These two
197 datasets both showed that the indicator $\frac{U}{R}$ could successfully capture the variability in annual
198 NEP.

199 **3.2 Local indicators for spatially varying NEP**

200 Across the 72 flux-tower sites, the across-site variation in mean annual NEP were significantly
201 correlated to mean annual $\ln\left(\frac{U}{R}\right)$ of each site ($R^2 = 0.65$, $P < 0.01$) (Fig. 3a). In this network,
202 the mean annual ratio $\ln\left(\frac{U}{R}\right)$ was a good indicator for cross-site variation in NEP. By contrast,
203 the spatial variation of IAV_{NEP} was moderately explained by the slope (i.e., β) of the temporal
204 correlation between NEP and $\ln\left(\frac{U}{R}\right)$ at each site ($R^2 = 0.39$, $P < 0.01$; Fig. 3b) rather than
205 $\ln\left(\frac{U}{R}\right)$ (Fig. S3). The wide range of ratio β reveals a large divergence of NEP sensitivity across
206 biomes, ranging from $121 \pm 118 \text{ g C m}^{-2} \text{ yr}^{-1}$ in shrubland to $473 \pm 112 \text{ g C m}^{-2} \text{ yr}^{-1}$ in cropland.

207 The decomposition of indicator $\frac{U}{R}$ into $\frac{\bar{U}}{\bar{R}}$ and $\frac{CUP}{CRP}$ allowed us to quantify the relative
208 importance of these two ratios in driving NEP variability. The linear regression and relative
209 importance analysis showed a more important role of $\frac{CUP}{CRP}$ (58%) than $\frac{\bar{U}}{\bar{R}}$ (42%) in explaining
210 the cross-site variation of NEP (Fig. 4). Therefore, the spatial distribution of mean annual NEP
211 was more strongly driven by the phenological changes.

212 **3.3 Simulated spatial variations in NEP by models**

213 We further used these two simple indicators (i.e., $\frac{U}{R}$ and β) to evaluate the simulated spatial
214 variations of NEP by the global flux tower-based product (i.e., FLUXCOM) and a widely-used
215 process-based model at the FLUXNET site level (i.e., CLM4.5). We found that the low spatial
216 variation of mean annual NEP in FLUXCOM and CLM4.5 could be inferred from their more
217 converging $\ln\left(\frac{U}{R}\right)$ than flux-tower measurements (Fig. 5). The underestimated variation of
218 IAV_{NEP} in these modeling results was also clearly shown by the smaller β values (268.22, 126.00
219 and 145.08 for FLUXNET, FLUXCOM and CLM4.5, respectively) (Fig. 5b).

220 In addition, the spatial variations of NEP and IAV_{NEP} were associated with the spatial
221 resolution of the product (Marcolla et al., 2017). Considering the scale mismatch between
222 FLUXNET sites and the gridded product, we run the same analysis at the global scale based on
223 Jena Inversion product. At the global scale, the spatial variation of mean annual NEP can be also
224 well indicated by $\ln\left(\frac{U}{R}\right)$ (Fig. 6). The larger net C uptake in FLUXCOM resulted from its
225 higher simulations for $\ln\left(\frac{U}{R}\right)$. Furthermore, the larger spatial variation of IAV_{NEP} in CLM4.5
226 could be inferred from the indicator β .

227 4. Discussion

228 4.1 New perspective for locating the major and sustainable land C sinks

229 Large spatial differences of mean annual NEP and IAV_{NEP} have been well-documented in
230 previous studies (Jung et al., 2017; Marcolla et al., 2017; Fu et al., 2019). Here we provide a
231 new perspective for quantifying the spatially varying NEP by tracing annual NEP into several
232 local indicators. Therefore, these traceable indicators could provide useful constraints for
233 predicting annual NEP, especially in areas without eddy-covariance towers.

234 Typically, the C sink capacity and its stability of a specific ecosystem are characterized
235 separately (Keenan et al., 2014; Ahlstrom et al., 2015; Jung et al., 2017). Here we integrated
236 NEP into two simple indicators that could directly locate the major and sustainable land C sink.
237 Among biomes, forests and croplands had the largest $\ln\left(\frac{U}{R}\right)$ and β , indicating the strongest and
238 the most unstable C sink in forests and croplands, respectively. However, the relatively lower β
239 in shrublands and savannas should be interpreted cautiously. There are very few semi-arid

240 ecosystems in the FLUXNET sites, while they represent a large portion of land at the global
241 scale and have been shown to substantially control the interannual variability of NEP (Ahlström
242 et al., 2015). The highest β implies that the land covered by cropland with the largest $I_{AV_{NEP}}$.
243 Therefore, the reported rapid global expansion of cropland may enlarge the fluctuations in Land-
244 atmosphere CO_2 exchange. In fact, the cropland expansion has been confirmed as one important
245 driver of the recent increasing global vegetation growth peak (Huang et al., 2018) and
246 atmospheric CO_2 seasonal amplitude (Gary et al., 2014; Zeng et al., 2014).

247 **4.2 Joint control of plant phenology and physiology on mean annual NEP**

248 Recent studies have demonstrated that the spatiotemporal variations in terrestrial gross primary
249 productivity are jointly controlled by plant phenology and physiology (Xia et al., 2015; Zhou et
250 al., 2016). Here we demonstrated that the spatial difference of mean annual NEP was determined
251 by both the phenology indicator $\frac{CUP}{CRP}$ (58%) and the physiological indicator $\frac{\bar{U}}{\bar{R}}$ (42%). In
252 addition, the lower contribution of the physiological indicator could partly be attributed to the
253 convergence of $\frac{\bar{U}}{\bar{R}}$ across FLUXNET sites (Fig. S4).

254 The convergent $\frac{\bar{U}}{\bar{R}}$ across sites was first discovered by Churkina *et al.* (2005) as 2.73 ± 1.08
255 across 28 sites, which included DBF, EBF and crop/grass. In this study, we found the $\frac{\bar{U}}{\bar{R}}$ across
256 the 72 sites is 2.71 ± 1.61 , which confirms with the findings of Churkina *et al.* This spatial
257 convergence of $\frac{\bar{U}}{\bar{R}}$ at site level provides important constraints for global models that simulate
258 large spatial variation in physiological processes (Peng et al., 2015; Xia et al., 2017). These
259 findings imply that the phenology changes will greatly affect the locations of the terrestrial
260 carbon sink by modifying the length of carbon uptake period (Richardson et al., 2013; Keenan
261 et al., 2014).

262 **4.3 The simulated local indicators from gridded products**

263 This study showed that the considerable spatial variations in mean annual NEP and $I_{AV_{NEP}}$ from
264 global gridded products could also be inferred from their local indicators. The low variations of
265 $\frac{U}{R}$ ratio in CLM4.5 could be largely due to their simple representations of the diverse terrestrial

266 plant communities into a few plant functional types with parameterized properties (Cui et al.,
267 2019; Sakschewski et al., 2015). In addition, the higher $\frac{U}{R}$ ratio from FLUXCOM product
268 indicated its widely reported larger net C uptake (Fig. 6) (Jung et al., 2020). Meanwhile, the
269 ignorance of fire, land-use change and other disturbances could lead to the smaller β by allowing
270 for only limited variations of phenological and physiological dynamics (Reichstein et al., 2014;
271 Kunstler et al., 2016). Although the magnitude of IAV_{NEP} depends on the spatial resolution
272 (Marcolla et al., 2017), we recommend future model benchmarking analyses to use not only the
273 global product compiled from machine-learning method (Bonan et al., 2018) but also the site-
274 level measurements or indicators (Xia et al., 2020).

275 **4.4 Conclusions and further implications**

276 In summary, this study highlights the changes in NEP and IAV_{NEP} over space on the land, and
277 provides the $\frac{U}{R}$ ratio and β as two simple local indicators for their spatial variations. These
278 indicators could be helpful for locating the persistent terrestrial C sinks in where the $\ln(\frac{U}{R})$
279 ratio is high but the β is low. Their estimates based on observations are also valuable for
280 benchmarking and improving the simulation of land-atmospheric C exchanges in Earth system
281 models. The findings in this study have some important implications for understanding the
282 variation of NEP on the land. First, forest ecosystems have the largest annual NEP due to the
283 largest $\ln(\frac{U}{R})$ while croplands show the highest IAV_{NEP} because of the highest β . Second, the
284 spatial convergence of $\frac{\bar{U}}{\bar{R}}$ suggests a tight linkage between plant growth and the non-growing
285 season soil microbial activities (Xia et al., 2014; Zhao et al., 2016). However, it remains unclear
286 whether the inter-biome variation in $\frac{\bar{U}}{\bar{R}}$ is due to different plant-microbe interactions between
287 biomes. Third, the within-site convergent but spatially varying β needs better understanding.
288 Previous studies have shown that a rising standard deviation of ecosystem functions could
289 indicate an impending ecological state transition (Carpenter and Brock, 2006; Scheffer et al.,
290 2009). Thus, a sudden shift of the β -value may be an important early-warning signal for the
291 critical transition of carbon uptake sensitivity of an ecosystem. In this study, the atmospheric
292 inversion product shows low correlation between NEP and $\ln(\frac{U}{R})$ in some boreal ecosystems,

293 which might due to that the terrestrial NEP is not well constrained for these regions or these
294 boreal ecosystems are experiencing state transition. Therefore, the robustness in relationship
295 between annual NEP and $\ln\left(\frac{U}{R}\right)$ depends on the temporal stability of carbon uptake sensitivity
296 for an ecosystem. In addition, the spatial variation in β reveals the differences of carbon uptake
297 sensitivity across ecosystems. Furthermore, considering the limited eddy-covariance sites with
298 long-term observations, these findings need further validation once the longer time-series of
299 measurements from more sites and vegetation types become available.

300 **Acknowledgements**

301 This work was financially supported by the National Key R&D Program of China
302 (2017YFA0604600), National Natural Science Foundation of China (31722009, 41630528),
303 National 1000 Young Talents Program of China, Shanghai Key Lab for Urban Ecological
304 Processes and Eco-Restoration (SHUES2020B01) and the Fundamental Research Funds for the
305 Central Universities. This work used eddy covariance dataset acquired and shared by the
306 FLUXNET community, including these networks: AmeriFlux, AfriFlux, AsiaFlux, CarboAfrica,
307 CarboEuropeIP, CarboItaly, CarboMont, ChinaFlux, Fluxnet-Canada, GreenGrass, ICOS,
308 KoFlux, LBA, NECC, OzFlux-TERN, TCOS-Siberia, and USCCC. The ERA-Interim
309 reanalysis data are provided by ECMWF and processed by LSCE. The FLUXNET eddy
310 covariance data processing and harmonization was carried out by the European Fluxes Database
311 Cluster, AmeriFlux Management Project, and Fluxdata project of FLUXNET, with the support
312 of CDIAC and ICOS Ecosystem Thematic Center, and the OzFlux, ChinaFlux and AsiaFlux
313 offices.

314 *Data availability statement.* Eddy flux data are available at
315 <http://fluxnet.fluxdata.org/data/fluxnet2015-dataset/>, and the data supporting the findings of this
316 study are available within the article and the Supplementary Information. The FLUXCOM NEP
317 product can be downloaded from the Data Portal of the Max Planck Institute for Biochemistry
318 (<https://www.bgc-jena.mpg.de/geodb/projects/Home.php>). The Jena CarboScope Inversion
319 product is available at <http://www.bgc-jena.mpg.de/CarboScope/?ID=s>.

320 *Author contribution.* E. Cui and J. Xia devised and conducted the analysis. Y. Luo, S. Niu, Y.
321 Wang and C. Bian provided critical feedback on the method and results. All authors contributed

322 to discussion of results and writing the paper.

323 *Competing interests.* The authors declare that there is no conflict of interest.

324 **FIGURES**

325 **Figure 1** Relationship between annual NEP and $\frac{U}{R}$ for 72 FLUXNET sites (of the form $NEP =$
326 $\beta \cdot \ln\left(\frac{U}{R}\right)$). a, Dependence of annual NEP on the ratio between total CO₂ exchanges during net
327 uptake (U) and release (R) periods (i.e., $\frac{U}{R}$). Each line represents one flux site with at least 5
328 years of observations. b, Conceptual figure for the decomposition framework introduced in this
329 study. Annual NEP can be quantitatively decomposed into the following indicators: $NEP =$
330 $U - R$. c, Distribution of the explanation of $\frac{U}{R}$ on temporal variability of NEP (R^2) for
331 FLUXNET sites.

332 **Figure 2** Relationship between annual NEP and $\frac{U}{R}$ for Jena Inversion product (of the form
333 $NEP = \beta \cdot \ln\left(\frac{U}{R}\right)$). The black box indicates the location of the sample.

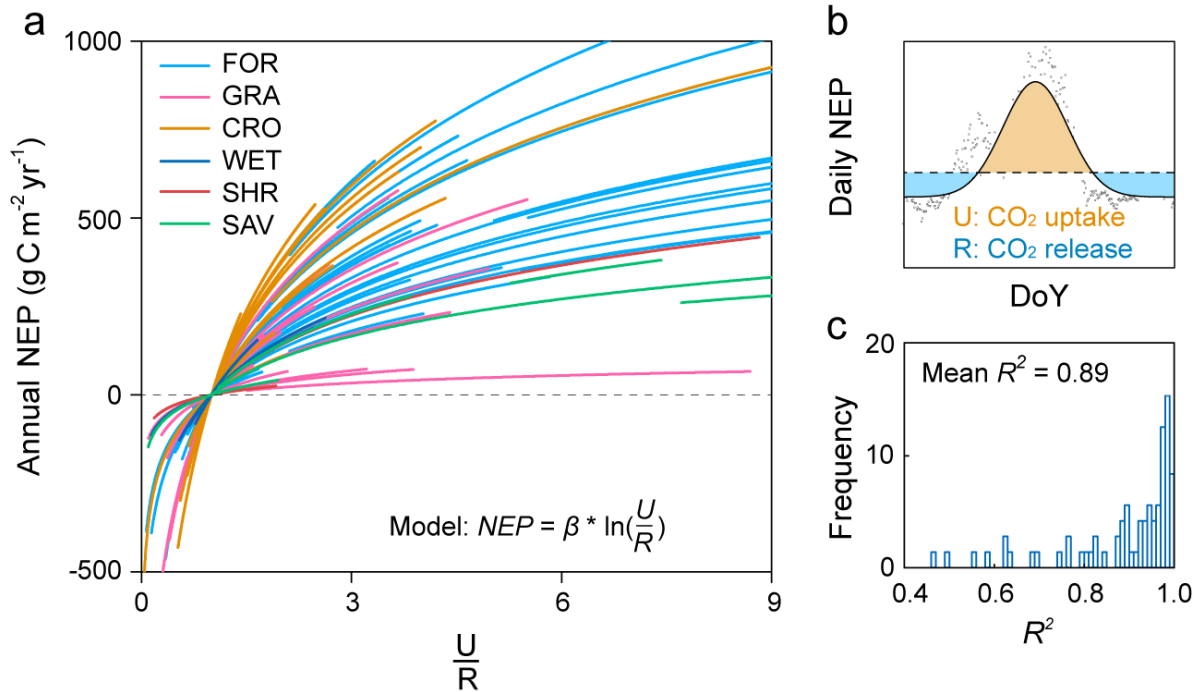
334 **Figure 3** Contributions of the two indicators in explaining the spatial patterns of mean annual
335 NEP and IAV_{NEP} . a, The relationship between annual mean NEP and $\ln\left(\frac{U}{R}\right)$ across FLUXNET
336 sites ($R^2 = 0.65, P < 0.01$). The insets show the variation of $\ln\left(\frac{U}{R}\right)$ for different terrestrial
337 biomes. b, The explanation of β on IAV_{NEP} ($R^2 = 0.39, P < 0.01$). The insets show the distribution
338 of parameter β for different terrestrial biomes. The number of site-years at each site is indicated
339 with the size of the point.

340 **Figure 4** The linear regression between $\frac{U}{R}$ with $\frac{CUP}{CRP}$ ($R^2 = 0.71, P < 0.01$) and $\frac{\bar{U}}{\bar{R}}$ ($R^2 = 0.09,$
341 $P < 0.01$) across sites. The insets show the relative contributions of each indicator to the spatial
342 variation of $\frac{U}{R}$. The number of site-years at each site is indicated with the size of the point.

343 **Figure 5** Representations of the spatially varying NEP and its local indicators in FLUXCOM
344 product and the Community Land Model (CLM4.5) at the FLUXNET site level. a, The variation
345 of mean annual NEP and IAV_{NEP} derives from FLUXNET, FLUXCOM and CLM4.5. Variation
346 in mean annual NEP: the standard deviation of mean annual NEP across sites; Variation in
347 IAV_{NEP} : the standard deviation of IAV_{NEP} across sites. b, Representations of the local indicators
348 for NEP in FLUXNET, FLUXCOM and CLM4.5. The corresponding distributions of $\ln\left(\frac{U}{R}\right)$
349 and β are shown at the top and right. Significance of the relationship between annual NEP and

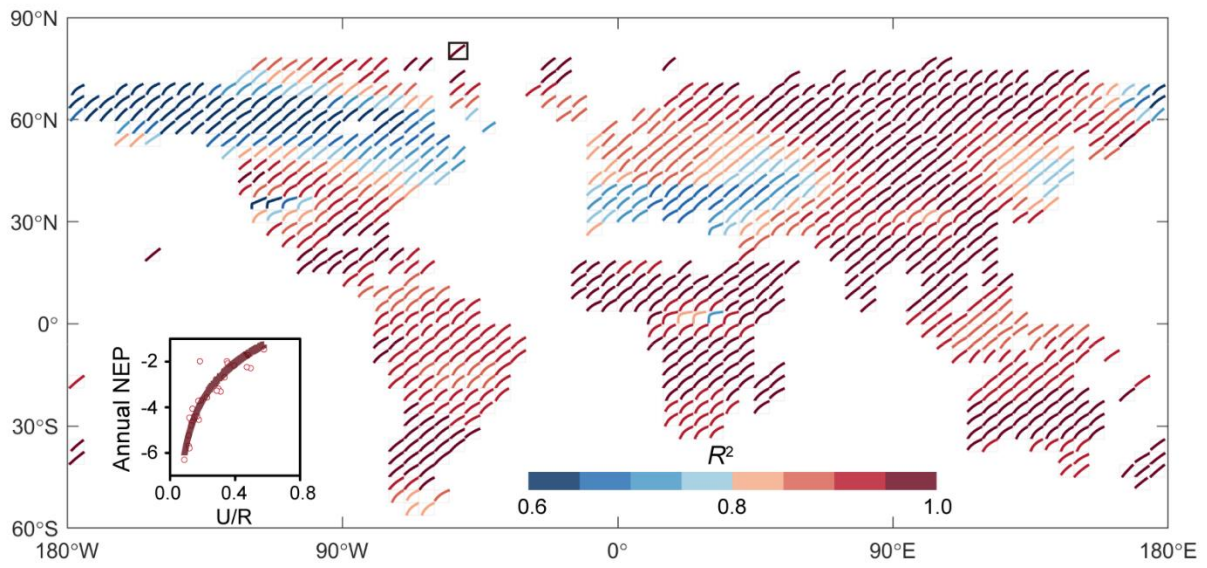
350 $\ln\left(\frac{U}{R}\right)$ for each site is indicated by the circle: closed circles: $P < 0.05$; open circles: $P > 0.05$. Note
351 that the modeled results are from the pixels extracted from the same locations of the flux tower
352 sites.

353 **Figure 6** Representations of the spatially varying NEP and its local indicators in FLUXCOM
354 product and the Community Land Model (CLM4.5) at the global scale. a, The variation of mean
355 annual NEP and $I_{AV_{NEP}}$ derives from Jena Inversion, FLUXCOM and CLM4.5. Variation in
356 mean annual NEP: the spatial variation of mean annual NEP; Variation in $I_{AV_{NEP}}$: the spatial
357 variation of standard deviation in $I_{AV_{NEP}}$. b, Representations of the local indicators for NEP in
358 Jena Inversion, FLUXCOM and CLM4.5.
359



360
 361 **Figure 1** Relationship between annual NEP and $\frac{U}{R}$ for 72 FLUXNET sites (of the form $NEP =$
 362 $\beta \cdot \ln\left(\frac{U}{R}\right)$). **a**, Dependence of annual NEP on the ratio between total CO₂ exchanges during net
 363 uptake (U) and release (R) periods (i.e., $\frac{U}{R}$). Each line represents one flux site with at least 5
 364 years of data. **b**, Conceptual figure for the decomposition framework introduced in this study.
 365 Annual NEP can be quantitatively decomposed into the following indicators: $NEP = U - R$. **c**,
 366 Distribution of the explanation of $\frac{U}{R}$ on temporal variability of FLUXNET NEP (R^2) for
 367 FLUXNET sites.

368

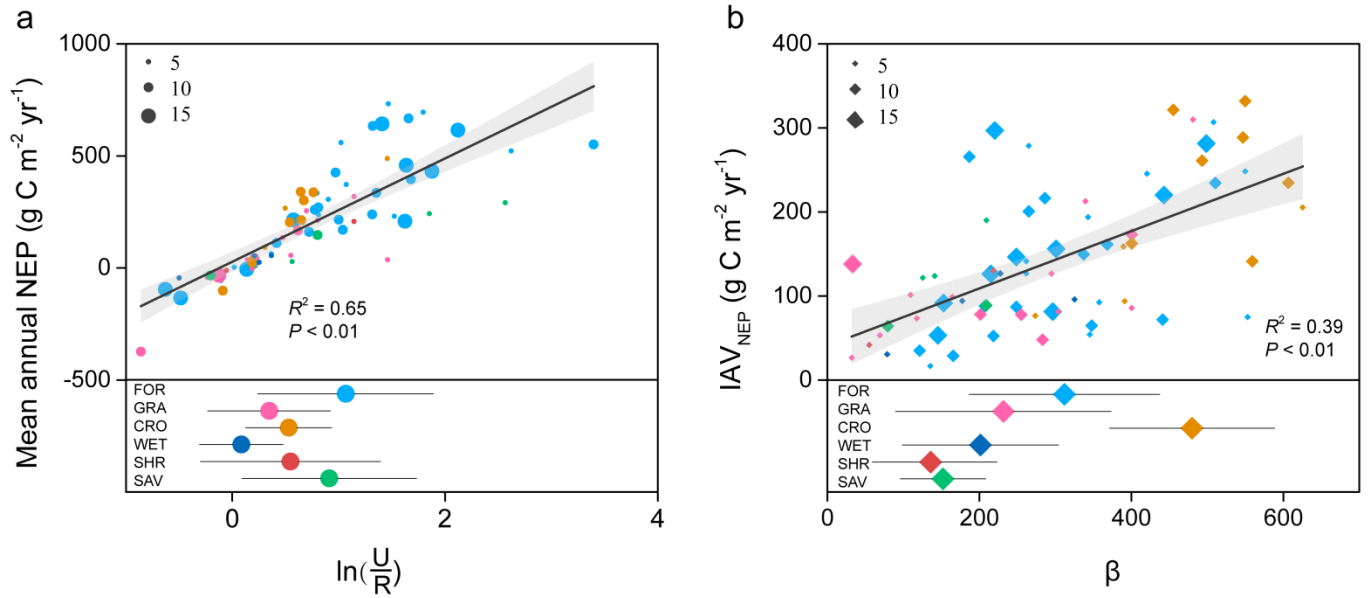


369

370 **Figure 2** Relationship between annual NEP and $\frac{U}{R}$ for Jena Inversion product (of the form

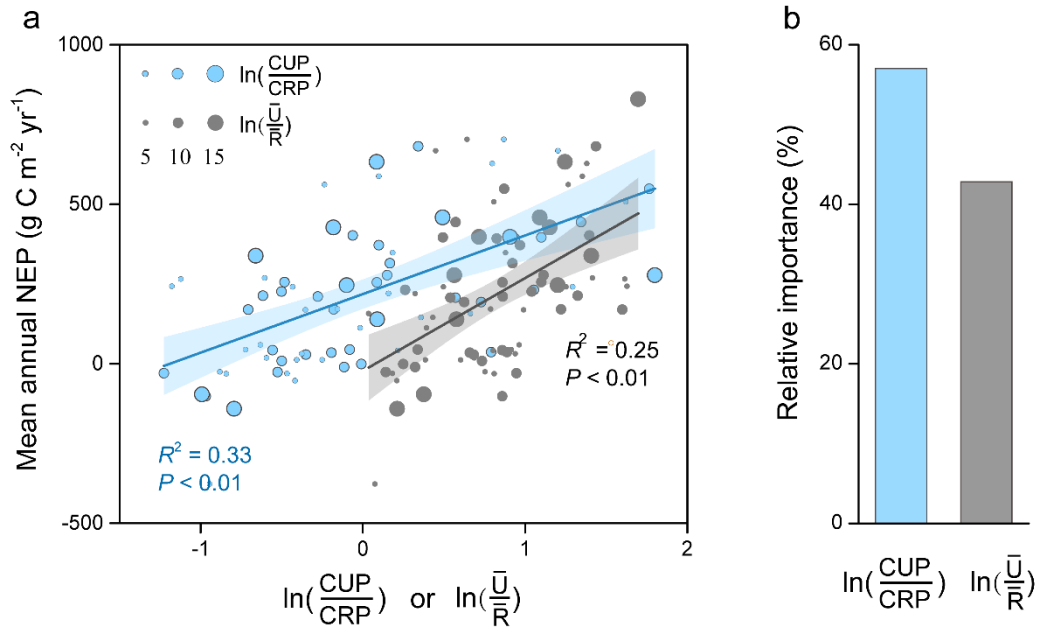
371 $NEP = \beta \cdot \ln\left(\frac{U}{R}\right)$). The black box indicates the location of the sample.

372

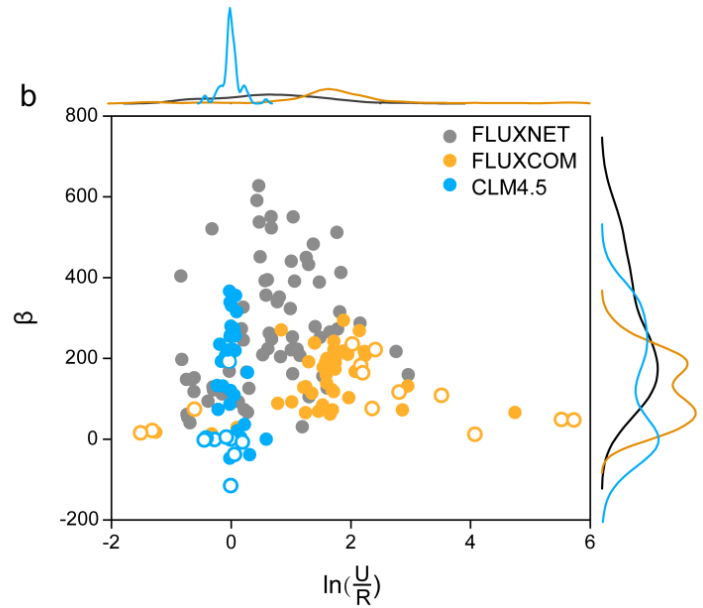
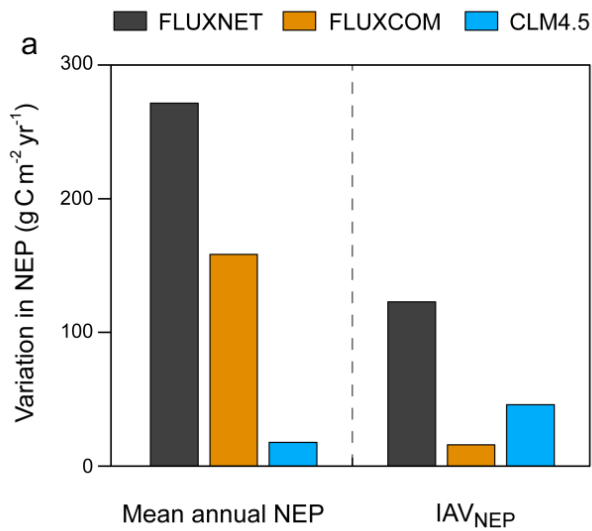


373
 374 **Figure 3** Contributions of the two indicators in explaining the spatial patterns of mean annual
 375 NEP and IAV_{NEP}. **a**, The relationship between annual mean NEP and $\ln(\frac{U}{R})$ across FLUXNET
 376 sites ($R^2 = 0.65$, $P < 0.01$). The insets show the variation of $\ln(\frac{U}{R})$ for different terrestrial
 377 biomes. **b**, The explanation of β on IAV_{NEP} ($R^2 = 0.39$, $P < 0.01$). The insets show the distribution
 378 of parameter β for different terrestrial biomes. The number of site-years at each site is indicated
 379 with the size of the point.

380



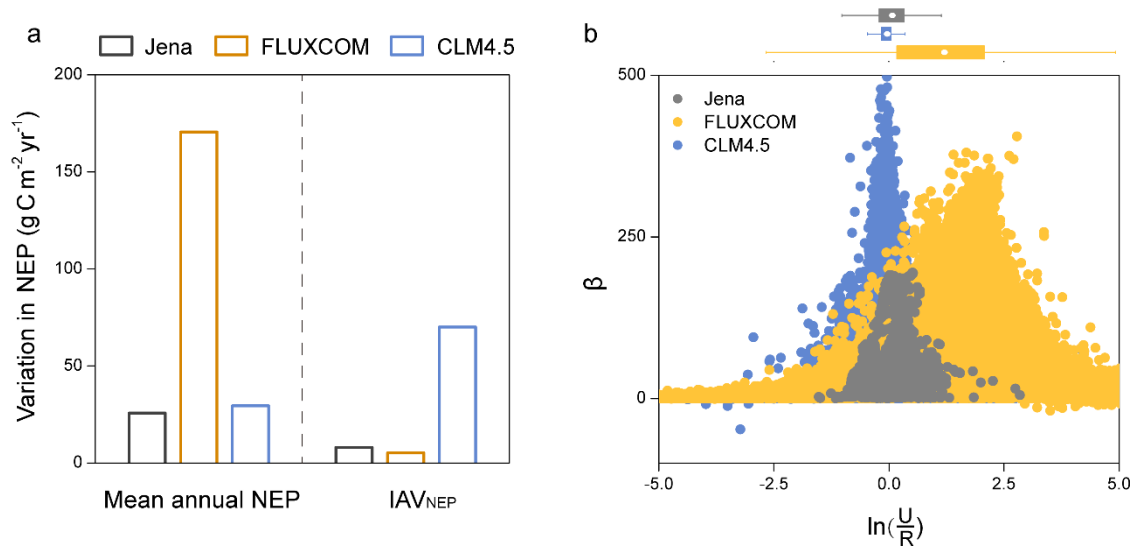
381
 382 **Figure 4** The relative contributions of the local indicators in explaining the spatial patterns of
 383 mean annual NEP. **a**, The linear regression between mean annual NEP with $\frac{CUP}{CRP}$ ($R^2 = 0.33$, P
 384 < 0.01) and $\frac{\bar{U}}{\bar{R}}$ ($R^2 = 0.25$, $P < 0.01$) across sites. **b**, The relative contributions of each indicator
 385 to the spatial variation of NEP. The number of site-years at each site is indicated with the size
 386 of the point.
 387



388

389 **Figure 5** Representations of the spatially varying NEP and its local indicators in FLUXCOM
 390 product and the Community Land Model (CLM4.5) at the FLUXNET site level. **a**, The variation
 391 of mean annual NEP and IAV_{NEP} derives from FLUXNET, FLUXCOM and CLM4.5. Variation
 392 in mean annual NEP: the standard deviation of mean annual NEP across sites; Variation in
 393 IAV_{NEP}: the standard deviation of IAV_{NEP} across sites. **b**, Representations of the local indicators
 394 for NEP in FLUXNET, FLUXCOM and CLM4.5. The corresponding distributions of $\ln\left(\frac{U}{R}\right)$
 395 and β are shown at the top and right. Significance of the relationship between annual NEP and
 396 $\ln\left(\frac{U}{R}\right)$ for each site is indicated by the circle: closed circles: $P < 0.05$; open circles: $P > 0.05$.
 397 Note that the modeled results are from the pixels extracted from the same locations of the flux
 398 tower sites.

399



400
 401 **Figure 6** Representations of the spatially varying NEP and its local indicators in FLUXCOM
 402 product and the Community Land Model (CLM4.5) at the global scale. a, The variation of mean
 403 annual NEP and IAV_{NEP} derives from Jena Inversion, FLUXCOM and CLM4.5. Variation in
 404 mean annual NEP: the spatial variation of mean annual NEP; Variation in IAV_{NEP}: the spatial
 405 variation of standard deviation in IAV_{NEP}. b, Representations of the local indicators for NEP in
 406 Jena Inversion, FLUXCOM and CLM4.5.

407

408 **References**

- 409 Ahlström, A., Raupach, M. R., Schurgers, G., Smith, B., Arneeth, A., Jung, M., Reichstein, M.,
410 Canadell, J. G., Friedlingstein, P., Jain, A. K., Kato, E., Poulter, B., Sitch, S., Stocker, B.
411 D., Viovy, N., Wang, Y., Wiltshire, A., Zaehle, S., and Zeng, N.: The dominant role of semi-
412 arid ecosystems in the trend and variability of the land CO₂ sink. *Science*, 348, 895-899,
413 2015.
- 414 Arora, V. K., Katavouta, A., Williams, R. G., Jones, C. D., Brovkin, V., Friedlingstein, P.,
415 Schwinger, J., Bopp, L., Boucher, O., Cadule, P., Chamberlain, M. A., Christian, J. R.,
416 Delire, C., Fisher, R. A., Hajima, T., Ilyina, T., Joetzjer, E., Kawamiya, M., Koven, C.,
417 Krasting, J., Law, R. M., Lawrence, D. M., Lenton, A., Lindsay, K., Pongratz, J., Raddatz,
418 T., Séférian, R., Tachiiri, K., Tjiputra, J. F., Wiltshire, A., Wu, T., and Ziehn, T.: Carbon-
419 concentration and carbon-climate feedbacks in CMIP6 models, and their comparison to
420 CMIP5 models, *Biogeosciences Discuss.*, <https://doi.org/10.5194/bg-2019-473>, in review,
421 2019.
- 422 Baldocchi, D., Chu, H., and Reichstein, M.: Inter-annual variability of net and gross ecosystem
423 carbon fluxes: A review. *Agric. For. Meteorol.*, 249, 520-533, 2018.
- 424 Baldocchi, D., Sturtevant, C., and Contributors, F.: Does day and night sampling reduce spurious
425 correlation between canopy photosynthesis and ecosystem respiration? *Agric. For.*
426 *Meteorol.*, 207, 117-126, 2015.
- 427 Besnard, S., Carvalhais, N., Arain, A., Black, A., de Bruin, S., Buchmann, N., Cescatti, A., Chen,
428 J., J.Clevers, J.G.P.W., Desai, A.R., Gough, C.M., Havrankova, K., Herold, M., Hörtnagl,
429 L., Jung, M., Knohl, A., Kruijt, B., Krupkova, L., Law, B.E., Lindroth, A., Noormets, A.,
430 Roupsard, O., Steinbrecher, R., Varlagin, A., Vincke, C. and Reichstein, M.: Quantifying
431 the effect of forest age in annual net forest carbon balance. *Environ. Res. Lett.*, 13, 124018,
432 2018.
- 433 Biederman, J. A., Scott, R. L., Goulden, M. L., Vargas, R., Litvak, M. E., Kolb, T. E., Yopez, E.
434 A., Oechel, W. C., Blanken, P. D., Bell, T. W., Garatuza-Payan, J., Maurer, . E., Dore, S.,
435 and Burns, S. P.: Terrestrial carbon balance in a drier world: the effects of water availability
436 in southwestern North America. *Glob. Change Biol.*, 22, 1867-1879, 2016.
- 437 Bonan, G. B., Patton, E. G., Harman, I. N., Oleson, K. W., Finnigan, J. J., Lu, Y., and Burakowski,
438 E. A.: Modeling canopy-induced turbulence in the Earth system: a unified parameterization
439 of turbulent exchange within plant canopies and the roughness sublayer (CLM-ml v0).
440 *Geosci. Model Dev.*, 11, 1467-1496, 2018.
- 441 Carpenter, S. R., and Brock, W. A.: Rising variance: a leading indicator of ecological transition.
442 *Ecol. Lett.*, 9, 311-318, 2006.
- 443 Churkina, G., Schimel, D., Braswell, B. H., and Xiao, X.: Spatial analysis of growing season
444 length control over net ecosystem exchange. *Glob. Change Biol.*, 11, 1777-1787, 2005.

445 Ciais, P., Tan, J., Wang, X., Roedenbeck, C., Chevallier, F., Piao, S. L., Moriarty, R., Broquet,
446 G., Le Quéré, C., Canadell, J. G., Peng, S., Poulter, B., Liu Z., and Tans, P.: Five decades
447 of northern land carbon uptake revealed by the interhemispheric CO₂ gradient. *Nature*, 568,
448 221-225, 2019.

449 Cui, E., Huang, K., Arain, M. A., Fisher, J. B., Huntzinger, D. N., Ito, A., Luo, Y., Jain, A. K.,
450 Mao, J., Michalak, A. M., Niu, S., Parazoo, N. C., Peng, C., Peng, S., Poulter, B., Ricciuto,
451 D. M., Schaefer, K. M., Schwalm, C. R., Shi, X., Tian, H., Wang, W., Wang, J., Wei, Y.,
452 Yan, E., Yan, L., Zeng, N., Zhu, Q., & Xia, J.: Vegetation functional properties determine
453 uncertainty of simulated ecosystem productivity: A traceability analysis in the East Asian
454 monsoon region. *Global Biogeochem. Cy.*, 33, 668-689, 2019.

455 Fu, Z., Dong, J., Zhou, Y., Stoy, P. C., and Niu, S.: Long term trend and interannual variability
456 of land carbon uptake-the attribution and processes. *Environ. Res. Lett.*, 12, 014018, 2017.

457 Fu, Z., Stoy, P. C., Poulter, B., Gerken, T., Zhang, Z., Wakkulcho, G., and Niu, S.: Maximum
458 carbon uptake rate dominates the interannual variability of global net ecosystem exchange.
459 *Glob. Change Biol.*, 25, 3381-3394, 2019.

460 Gilmanov, T. G., Tieszen, L. L., Wylie, B. K., Flanagan, L. B., Frank, A. B., Haferkamp, M. R.,
461 Meyers, T. P., and Morgan, J. A.: Integration of CO₂ flux and remotely-sensed data for
462 primary production and ecosystem respiration analyses in the Northern Great Plains:
463 Potential for quantitative spatial extrapolation. *Global Ecol. Biogeogr.*, 14, 271-292, 2005.

464 Gray, J. M., Frohling, S., Kort, E. A., Ray, D. K., Kucharik, C. J., Ramankutty, N., and Friedl,
465 M. A.: Direct human influence on atmospheric CO₂ seasonality from increased cropland
466 productivity. *Nature*, 515, 398-401, 2014.

467 Grömping, U.: Estimators of relative importance in linear regression based on variance
468 decomposition. *Am. Stat.*, 61, 139-147, 2007.

469 Huang, K., Xia, J., Wang, Y., Ahlström, A., Chen, J., Cook, R. B., Cui, E., Fang, Y., Fisher, J. B.,
470 Huntzinger, D. N., Li, Z., Michalak, A. M., Qiao, Y., Schaefer, K., Schwalm, C., Wang, J.,
471 Wei, Y., Xu, X., Yan, L., Bian C., and Luo, Y.: Enhanced peak growth of global vegetation
472 and its key mechanisms. *Nat. Ecol. Evol.*, 2, 1897-1905, 2018.

473 Jung, M., Reichstein, M., Schwalm, C. R., Huntingford, C., Sitch, S., Ahlström, A., Arneeth, A.,
474 Camps-Valls, G., Ciais, P., Friedlingstein, P., Gans, F., Ichii, K., Jain, A. K., Kato, E., Papale,
475 D., Poulter, B., Raduly, B., Rödenbeck, C., Tramontana, G., Viovy, N., Wang, Y., Weber,
476 U., Zaehle S., and Zeng, N.: Compensatory water effects link yearly global land CO₂ sink
477 changes to temperature. *Nature*, 541, 516-520, 2017.

478 Jung, M., Schwalm, C., Migliavacca, M., Walther, S., Camps-Valls, G., Koirala, S., Anthoni, P.,
479 Besnard, S., Bodesheim, P., Carvalhais, N., Chevallier, F., Gans, F., Goll, D. S., Haverd, V.,
480 Köhler, P., Ichii, K., Jain, A. K., Liu, J., Lombardozzi, D., Nabel, J. E. M. S., Nelson, J. A.,
481 O'Sullivan, M., Pallandt, M., Papale, D., Peters, W., Pongratz, J., Rödenbeck, C., Sitch, S.,
482 Tramontana, G., Walker, A., Weber, U., and Reichstein, M.: Scaling carbon fluxes from
483 eddy covariance sites to globe: synthesis and evaluation of the FLUXCOM approach,

484 Biogeosciences, 17, 1343-1365, 2020.

485 Keenan, T. F., Gray, J., Friedl, M. A., Toomey, M., Bohrer, G., Hollinger, D. Y., Munger, J. W.,
486 O’Keefe, J., Schmid, H. P., Wing, I. S., Yang, B., and Richardson, A. D.: Net carbon uptake
487 has increased through warming-induced changes in temperate forest phenology. *Nat. Clim.*
488 *Change*, 4, 598-604, 2014.

489 Kunstler, G., Falster, D., Coomes, D. A., Hui, F., Kooyman, R. M., Laughlin, D. C., Poorter, L.,
490 Vanderwel, M., Vieilledent, G., Wright, S. J., Aiba, M., Baraloto, C., Caspersen, J.,
491 Cornelissen, J. H. C., Gourlet-Fleury, S., Hanewinkel, M., Herault, B., Kattge, J.,
492 Kurokawa, H., Onoda, Y., Peñuelas, J., Poorter, H., Uriarte, M., Richardson, S., Ruiz-
493 Benito, P., Sun, I., Ståhl, G., Swenson, N. G., Thompson, J., Westerlund, B., Wirth, C.,
494 Zavala, M. A., Zeng, H., Zimmerman, J. K., Zimmermann N. E., and Westoby, M.: Plant
495 functional traits have globally consistent effects on competition. *Nature*, 529, 204-207,
496 2016.

497 Le Quéré, C., Andrew, R. M., Friedlingstein, P., Sitch, S., Hauck, J., Pongratz, J., Pickers, P. A.,
498 Korsbakken, J. I., Peters, G. P., Canadell, J. G., Arneeth, A., Arora, V. K., Barbero, L., Bastos,
499 A., Bopp, L., Chevallier, F., Chini, L. P., Ciais, P., Doney, S. C., Gkritzalis, T., Goll, D. S.,
500 Harris, I., Haverd, V., Hoffman, F. M., Hoppema, M., Houghton, R. A., Hurtt, G., Ilyina,
501 T., Jain, A. K., Johannessen, T., Jones, C. D., Kato, E., Keeling, R. F., Goldewijk, K. K.,
502 Landschützer, P., Lefèvre, N., Lienert, S., Liu, Z., Lombardozzi, D., Metzl, N., Munro, D.
503 R., Nabel, J. E. M. S., Nakaoka, S., Neill, C., Olsen, A., Ono, T., Patra, P., Peregón, A.,
504 Peters, W., Peylin, P., Pfeil, B., Pierrot, D., Poulter, B., Rehder, G., Resplandy, L.,
505 Robertson, E., Rocher, M., Rödenbeck, C., Schuster, U., Schwinger, J., Séférian, R.,
506 Skjelvan, I., Steinhoff, T., Sutton, A., Tans, P. P., Tian, H., Tilbrook, B., Tubiello, F. N., van
507 der Laan-Luijkx, I. T., van der Werf, G. R., Viovy, N., Walker, A. P., Wiltshire, A. J., Wright,
508 R., Zaehle, S., and Zheng, B.: Global carbon budget 2018. *Earth Syst. Sci. Data*, 10, 405,
509 2018.

510 Li, G., Han, H., Du, Y., Hui, D., Xia, J., Niu, S., Li, X., and Wan, S.: Effects of warming and
511 increased precipitation on net ecosystem productivity: a long-term manipulative
512 experiment in a semiarid grassland. *Agric. For. Meteorol.*, 232, 359-366, 2017.

513 Luo, Y., and Weng, E.: Dynamic disequilibrium of the terrestrial carbon cycle under global
514 change. *Trends Ecol. Evol.*, 26, 96-104, 2011.

515 Luo, Y., and Zhou, X.: *Soil respiration and the environment*. Elsevier, 2006.

516 Marcolla, B., Rödenbeck, C., and Cescatti, A.: Patterns and controls of inter-annual variability
517 in the terrestrial carbon budget. *Biogeosciences*, 14, 3815-3829, 2017.

518 Musavi, T., Migliavacca, M., Reichstein, M., Kattge, J., Wirth, C., Black, T. A., Janssens, I.,
519 Knohl, A., Loustau, D., Roupsard, O., Varlagin, A., Rambal, S., Cescatti, A., Gianelle, D.,
520 Kondo, H., Tamrakar, R., and Mahecha, M. D.: Stand age and species richness dampen
521 interannual variation of ecosystem-level photosynthetic capacity. *Nat. Ecol. Evol.*, 1, 0048,
522 2017.

523 Niu, S., Fu, Z., Luo, Y., Stoy, P. C., Keenan, T. F., Poulter, B., Zhang, L., Piao, S., Zhou, X.,
524 Zheng, H., Han, J., Wang, Q., and Yu, G.: Interannual variability of ecosystem carbon
525 exchange: From observation to prediction. *Global Ecol. Biogeogr.*, 26, 1225-1237, 2017.

526 Novick, K. A., Oishi, A. C., Ward, E. J., Siqueira, M. B., Juang, J. Y., and Stoy, P. C.: On the
527 difference in the net ecosystem exchange of CO₂ between deciduous and evergreen forests
528 in the southeastern United States. *Glob. Change Biol.*, 21, 827-842, 2015.

529 Oleson, K. W., Lawrence, D. M., Bonan, G. B., Drewniak, B., Huang, M., Koven, C. D., Levis,
530 S., Li, F., Riley, W. J., Subin, Z. M., Swenson, S. C., Thornton, P. E., Bozbiyik, A., Fisher,
531 R., Heald, C. L., Kluzek, E., Lamarque, J.-F., Lawrence, P. J., Leung, L. R., Lipscomb, W.,
532 Muszala, S., Ricciuto, D. M., Sacks, W., Sun, Y., Tang, J., and Yang, Z.-L.: Technical
533 description of version 4.5 of the Community Land Model (CLM), NCAR Earth System
534 Laboratory-Climate and Global Dynamics Division, Boulder, Colorado, USA, Tech. Rep.
535 TN-503+STR, http://www.cesm.ucar.edu/models/cesm1.2/clm/CLM45_Tech_Note.pdf
536 (last access: 27 September 2017), 2013.

537 Pastorello, G., Papale, D., Chu, H., Trotta, C., Agarwal, D., Canfora, E., Baldocchi, D., and Torn,
538 M.: A new data set to keep a sharper eye on land-air exchanges. *Eos*, 98, 2017.

539 Peng, S., Ciais, P., Chevallier, F., Peylin, P., Cadule, P., Sitch, S., Piao, S., Ahlström, A.,
540 Huntingford, C., Levy, P., Li, X., Liu, Y., Lomas, M., Poulter, B., Viovy, N., Wang, T.,
541 Wang, X., Zaehle, S., Zeng, N., Zhao, F., and Zhao, H.: Benchmarking the seasonal cycle
542 of CO₂ fluxes simulated by terrestrial ecosystem models. *Global Biogeochem. Cy.*, 29, 46-
543 64, 2015.

544 Peylin, P., Law, R. M., Gurney, K. R., Chevallier, F., Jacobson, A. R., Maki, T., Niwa, Y., Patra,
545 P. K., Peters, W., Rayner, P. J., Rödenbeck, C., van der Laan-Luijkx, I. T., and Zhang, X.:
546 Global atmospheric carbon budget: results from an ensemble of atmospheric CO₂
547 inversions. *Biogeosciences*, 10, 6699-6720, 2013.

548 Poulter, B., Frank, D., Ciais, P., Myneni, R. B., Andela, N., Bi, J., Broquet, G., Canadell, J. G.,
549 Chevallier, F., Liu, Y. Y., Running, S. W., Sitch, S., and van der Werf, G. R.: Contribution
550 of semi-arid ecosystems to interannual variability of the global carbon cycle. *Nature*, 509,
551 600-603, 2014.

552 Randerson, J. T.: Climate science: Global warming and tropical carbon. *Nature*, 494, 319-320,
553 2013.

554 Randerson, J. T., Chapin III, F. S., Harden, J. W., Neff, J. C., and Harmon, M. E.: Net ecosystem
555 production: a comprehensive measure of net carbon accumulation by ecosystems. *Ecol.*
556 *Appl.*, 12, 937-947, 2002.

557 R Development Core Team.: R: A Language and Environment for Statistical Computing 3-
558 900051-07-0, R Foundation for Statistical Computing, Vienna, Austria, 2011.

559 Reichstein, M., Bahn, M., Mahecha, M. D., Kattge, J., and Baldocchi, D. D.: Linking plant and
560 ecosystem functional biogeography. *Proc. Natl Acad. Sci. USA*, 111, 13697-13702, 2014.

561 Reichstein, M., Falge, E., Baldocchi, D., Papale, D., Aubinet, M., Berbigier, P., Bernhofer, C.,

562 Buchmann, N., Gilmanov, T., Granier, A., Grünwald, T., Havránková, K., Ilvesniemi, H.,
 563 Janous, D., Knohl, A., Laurila, T., Lohila, A., Loustau, D., Matteucci, G., Meyers, T.,
 564 Miglietta, F., Ourcival, J., Pumpanen J., Rambal, S., Rotenberg, E., Sanz, M., Tenhunen,
 565 J., Seufert, G., Vaccari, F., Vesala, T., Yakir, D., and Valentini, R.: On the separation of net
 566 ecosystem exchange into assimilation and ecosystem respiration: review and improved
 567 algorithm. *Glob. Change Biol.*, 11, 1424-1439, 2005.

568 Richardson, A. D., Keenan, T. F., Migliavacca, M., Ryu, Y., Sonnentag, O., and Toomey, M.:
 569 Climate change, phenology, and phenological control of vegetation feedbacks to the
 570 climate system. *Agric. For. Meteorol.*, 169, 156-173, 2013.

571 Rödenbeck, C., Zaehle, S., Keeling, R., and Heimann, M.: How does the terrestrial carbon
 572 exchange respond to inter-annual climatic variations? *Biogeosciences*, 15, 2481-2498,
 573 2018.

574 Sakschewski, B., von Bloh, W., Boit, A., Rammig, A., Kattge, J., Poorter, L., Peñuelas, J., and
 575 Thonicke, K.: Leaf and stem economics spectra drive diversity of functional plant traits in
 576 a dynamic global vegetation model. *Glob. Change Biol.*, 21, 2711-2725, 2015.

577 Scheffer, M., Bascompte, J., Brock, W. A., Brovkin, V., Carpenter, S. R., Dakos, V., Held, H.,
 578 van Nes, E. H., Rietkerk, M., and Sugihara, G.: Early-warning signals for critical transitions.
 579 *Nature*, 461, 53-59, 2009.

580 Valentini, R., Matteucci, G., Dolman, A. J., Schulze, E. D., Rebmann, C. J. M. E. A. G., Moors,
 581 E. J., Granier, A., Gross, P., Jensen, N. O., Pilegaard, K., Lindroth, A., Grelle, A., Bernhofer,
 582 C., Grünwald, T., Aubinet, M., Ceulemans, R., Kowalski, A. S., Vesala, T., Rannik, Ü.,
 583 Berbigier, P., Loustau, D., Guðmundsson, J., Thorgeirsson, H., Ibrom, A., Morgenstern, K.,
 584 Clement, R., Moncrieff, J., Montagnani, L., Minerbi S., and Jarvis, P. G.: Respiration as
 585 the main determinant of carbon balance in European forests. *Nature*, 404, 861-865, 2000.

586 Von Buttlar, J., Zscheischler, J., Rammig, A., Sippel, S., Reichstein, M., Knohl, A., Jung, M.,
 587 Menzer, O., Arain, M., Buchmann, N., Cescatti, A., Geinelle, D., Kiely, G., Law, B.,
 588 Magliudo, V., Margolis, H., McCaughey, H., Merbold, L., Migliavacca, M., Montagnani,
 589 L., Oechel, W., Pavelka, M., Pelchl, M., Rambal, S., Raschi, A., Scott, R.L., Vaccari, F.,
 590 Van Gorsel, E., Varlagin, A., Wohlfahrt, G., and Mahecha, M.: Impacts of droughts and
 591 extreme temperature events on gross primary production and ecosystem respiration: a
 592 systematic assessment across ecosystems and climate zones. *Biogeosciences*, 15, 1293-
 593 1318, 2017.

594 Xia, J., Chen, J., Piao, S., Ciais, P., Luo, Y., and Wan, S.: Terrestrial carbon cycle affected by
 595 non-uniform climate warming. *Nat. Geosci.*, 7, 173-180, 2014.

596 Xia, J., McGuire, A. D., Lawrence, D., Burke, E., Chen, G., Chen, X., Delire, C., Koven, C.,
 597 MacDougall, A., Peng, S., Rinke, A., Saito, K., Zhang, W., Alkama, R., Bohn, T. J., Ciais,
 598 P., Decharme, B., Gouttevin, I., Hajima, T., Hayes, D. J., Huang, K., Ji, D., Krinner, G.,
 599 Lettenmaier, D. P., Miller, P. A., Moore, J. C., Smith, B., Sueyoshi, T., Shi, Z., Yan, L.,
 600 Liang, J., Jiang, L., Zhang, Q., and Luo, Y.: Terrestrial ecosystem model performance in

601 simulating productivity and its vulnerability to climate change in the northern permafrost
602 region. *J. Geophys. Res-Bioge.*, 122, 430-446, 2017.

603 Xia, J., Niu, S., Ciais, P., Janssens, I. A., Chen, J., Ammann, C., Arain, A., Blanken, P. D.,
604 Cescatti, A., Bonal, D., Buchmann, N., Curtis, P. S., Chen, S., Dong, J., Flanagan, L. B.,
605 Frankenberg, C., Georgiadis, T., Gough, C. M., Hui, D., Kiely, G., Li, J., Lund, M.,
606 Magliulo, V., Marcolla, B., Merbold, L., Montagnani, L., Moors, E. J., Olesen, J. E., Piao,
607 S., Raschi, A., Rouspard, O., Suyker, A. E., Urbaniak, M., Vaccari, F. P., Varlagin, A.,
608 Vesala, T., Wilkinson, M., Weng, E., Wohlfahrt, G., Yan, L., and Luo, Y.: Joint control of
609 terrestrial gross primary productivity by plant phenology and physiology. *Proc. Natl Acad.*
610 *Sci. USA*, 112, 2788-2793, 2015.

611 Xia, J., Wang, J., and Niu, S.: Research challenges and opportunities for using big data in global
612 change biology. *Glob. Change Biol.*, 2020. <https://doi.org/10.1111/gcb.15317>

613 Yu, G., Chen, Z., Piao, S., Peng, C., Ciais, P., Wang, Q., Li, X., and Zhu, X.: High carbon dioxide
614 uptake by subtropical forest ecosystems in the East Asian monsoon region. *Proc. Natl Acad.*
615 *Sci. USA*, 111, 4910-4915, 2014.

616 Zeng, N., Zhao, F., Collatz, G. J., Kalnay, E., Salawitch, R. J., West, T. O., and Guanter, L.:
617 Agricultural Green Revolution as a driver of increasing atmospheric CO₂ seasonal
618 amplitude. *Nature*, 515, 394-397, 2014.

619 Zhao, J., Peichl, M., Öquist, M., and Nilsson, M. B.: Gross primary production controls the
620 subsequent winter CO₂ exchange in a boreal peatland. *Glob. Change Biol.*, 22, 4028-4037,
621 2016.

622 Zhou, S., Zhang, Y., Ciais, P., Xiao, X., Luo, Y., Caylor, K. K., Huang, Y., and Wang, G.:
623 Dominant role of plant physiology in trend and variability of gross primary productivity in
624 North America. *Sci. Rep.*, 7, 41366, 2017.

625